International Journal of Control, Automation and Systems 16(X) (2018) 1-12
http://dx.doi.org/10.1007/s12555-017-0154-7
ISSN:1598-6446 eISSN:2005-4092
http://www.springer.com/12555

Sensorless Reaction Force Estimation of the End Effector of a Dual-arm Robot Manipulator Using Sliding Mode Control with a Sliding Perturbation Observer

Karam Dad Kallu, Wang Jie, and Min Cheol Lee*

Abstract: We estimated the reaction force for assembly work with a three-link dual-arm robot manipulator using sliding mode control with a sliding perturbation observer (SMCSPO) without using a force sensor. The sliding perturbation observer (SPO) is used to estimate the reaction force of the end effector without using any sensor. The SPO estimates the perturbation, which consists of the parameter uncertainties, nonlinear terms, and disturbances such as the reaction force. During assembly, the most effective perturbation term is close to the reaction force, so we assumed that the estimated perturbation is the same as the reaction force. The estimated perturbation was compared with the reaction force from the dynamics of the manipulator using a simulation with the SimMechanics toolbox of MATLAB/SIMULINK. The simulation results show the performance of the SMCSPO and that the reaction force can be estimated using the SPO without any sensor. The method can improve the structural reduction of link manipulator robots and decrease costs.

Keywords: Estimated perturbation, manipulator, reaction force, SMCSPO.

1. INTRODUCTION

Estimation of the reaction force of the end effector of a link manipulator can be useful in many robotic applications that involve physical contact between the robot and environment without using any sensors. Estimating the reaction force can reduce the costs needed for sensors. Many robotic tasks require the end effector of the robot to establish and maintain contact with the environment, such as deburring, welding, grinding, precision assembly, and various industrial processes. For successful execution of such tasks, both force control and position control of the robot manipulator must be performed simultaneously.

However, force control is not popular in industrial applications due to the high price of the sensors and the lack of appropriate control algorithms. Moreover, a force sensor cannot be used when the robot manipulator is affected by environmental uncertainties, such as high temperature and high noise. Several force estimation methods have been reported to overcome these problems [1–4].

Force estimation for robotic manipulators has been a topic of interest since the early 1990s. An approach based on a decoupled disturbance observer was proposed [5]. Hacksel and Salcudean presented a coupled-force observer based on accurate knowledge of the robot's dynamics [6]. Both observer-based approaches demonstrated good results with direct drive manipulators with negligible friction dynamics. Dynamic learning has been used in force estimation. One study used a neural network to learn the entire dynamical model of a 3-degree-of-freedom (DOF) haptic device offline [7]. Their system had little friction. Another study demonstrated force-sensorless hybrid force/position control [8]. They used a simplified model of the robot dynamics, which consisted of a gravity term and learned friction terms. Adaptive neural networks were used for online friction learning, but adaptation of the modeled dynamics was not performed.

Motor current was used to estimate external forces for robots with harmonic drive gearing [9]. To determine the estimated external torque, the approach involved subtracting the modeled dynamics from the motor torque, which is assumed to be proportional to the motor current. The estimated torque contained significant unmodeled position-dependent friction. Filtering the estimated external torque in the position domain greatly improved the estimates. However, the filtering was done offline, and the entire po-

Manuscript received March 26, 2017; revised September 1, 2017; accepted November 27, 2017. Recommended by Associate Editor Kyoungchul Kong under the direction of Editor Yoshito Ohta. This work was supported by the National Research Foundation of Korea (NRF) grant funded by the Korea Government (MSIP)(No.NRF-2012M2B2B 1055503) This research was supported by The Technology Innovation Program(10073147, Development of Robot Manipulation Technology by Using Artificial Intelligence) funded By the Ministry of Trade, Industry & Energy.

Karam Dad Kallu, Wang Jie, and Min Cheol Lee are with the Department of Mechanical Engineering, Pusan National University, 635-4 Jangjeon-2 dong, Geumjeong-gu, Busan 46241, Korea (e-mails: karamdadkallu@gmail.com, wangjie@pusan.ac.kr, mclee@pusan.ac.kr).
* Corresponding author.

sition history of the estimated external torque was known.

Another approach performed end effector force estimation based on noisy actuator torque measurements [10]. Two methods were presented, and the first one uses a filtered dynamic model and a recursive least-squares estimation with exponential forgetting to estimate the force. The second estimation approach is based on a generalized momentum-based disturbance observer. Experiments were performed using a 2-DOF manipulator with pneumatic muscle actuators. The end effector forces in the x and y directions were estimated successfully in a range of within forces between ± 6 N, despite of despite the noise.

Another study proposed real-time estimation of the contact location and contact force along a planar joint robot manipulator without using external sensory systems [11]. To estimate the contact location and contact force based on external joint torques, global optimization and local optimization were combined [12]. An algorithm was used to estimate external forces exerted on the end effector of a robot manipulator using information from joint torque sensors [13]. A novel algorithm was presented for simultaneous force estimation and friction compensation of the constrained motion of robot manipulators [14]. Another study proposed a non-linear observer to estimate the state (position and velocity) of links and external forces exerted by the robot during friction stir welding [15].

A force estimator was introduced for force-sensorless robotic manipulators [16]. The algorithm is based on knowledge of the dynamics of the robotic device, but the mass of the load is typically unknown. A method was developed to estimate the reaction force of a surgical robot instrument without sensors, and a state observer control algorithm was used [17]. An SPO-based reaction force estimation method was used to extract the pure reaction force on a surgical robot instrument including Coulomb friction due to the operation of a cable-pulley structure [18].

A robust force estimation algorithm was proposed for estimating the 3D contact force acting on a three-link robot manipulator [19]. The algorithm was developed by combining an extended Kalman filter with an adaptive law for non-linear stochastic systems with unknown inputs. To test the theory, simulations were performed, and the joint positions and velocities of a three-link manipulator are used as measurements. Variable-structure sliding mode control (SMC) has been used extensively use since the paper by Utkin [20]. In this control method, the states of the system are directed to reach a predefined sliding surface, where they are maintained by means of a sliding motion. While sliding, the system is insensitive to parameter variations and external disturbances. Due to the robust behavior of SMC, it has many applications in industry, such as robotic manipulator control [21, 22], control of mobile robots [23, 24], process control [25], and flight control [26].

Output feedback-based distributed adaptive consensus control was developed for multi-agent systems with Lipschitz non-linear dynamics [27]. New control approaches were presented for synchronization of master and slave chaotic systems by means of novel coupled chaotic synchronous observers and coupled chaotic adaptive synchronous observers [28]. A method requiring less computational effort was also proposed for solving matrix inequalities to obtain the observer and controller gain matrices using a decoupling technique. An observer based controller design was presented for a class of nonlinear systems with time-varying parametric uncertainties and norm-bounded disturbances [29]. Observer-based controller design was described for one-sided Lipschitz nonlinear systems [30]. An observer-based controller design condition was obtained by the application of Lyapunov theory.

In the area of robotics, observers can be used to obtain improved position tracking control of manipulators by providing accurate joint velocity estimates without the use of tachometers. A nonlinear model-based joint rate observer for serial kinematic mechanisms has been presented [31]. A model-based observer was used with sliding-mode control of a robot to show good position trajectory tracking [32]. Motivated by the need to accurately control a magnetically levitated wrist for precision assembly [33, 34], active vibration control [35], and tele-operation [36]. A model-based approach was also used to design an angular-velocity observer for rigid body motion [37]. In order to produce small error, the rigid-body motion velocity observers developed so far require accurate plant models. This includes small errors in the mass parameters and the absence of unmodeled dynamics, environment forces, and torques. In the case of direct-drive robots, the plant model can be very accurate, provided that the robot mass parameters are identified [38].

Dual-arm cooperative robot systems are used in a wide range of industrial applications. These systems are able to handle large objects and assemble complex industrial parts with high precision and reliability, such as in the production of metal sheet profiles and welding with heavy machinery on production lines [39–41]. Dual-arm robotic systems are frequently preferred for hazardous tasks, such as transportation of active uranium in nuclear power plants or disposal of explosive ordnance [42]. A dual-arm robot is more advantageous than single-arm versions due to the lower joint torque requirement for the same task. A dual-arm robot manipulator needs vision sensors and a recognition algorithm for tasks such as selection, picking, assembly work, or distinguishing some defects [43]. Despite these advantages, robot manipulators cannot assemble parts as well as like humans do. The most important sense other than vision is touch when a manipulator assembles a part, so force sensors are needed for accurate operating. But attaching a force sensor to the end effector

of a manipulator is difficult because of the weight, cost, and structural problems.

To overcome these problems, this study introduces a design method to estimate the reaction force on the end effector of a three-link dual-arm robot without using any force sensors. SMCSPO is used to control the manipulator, where the SPO computes the quantity of the estimated perturbation, which is a combination of the uncertainties, nonlinear terms, and disturbances such as the reaction force. During assembly tasks or collisions, the most effective perturbation term is assumed to be the reaction or collision force because each joint's nonlinear dynamics is going to small due to reduced velocity at contact or collision instant but assembly or collision forces are increasing.

The rest of the paper is organized as follows: Section 2 describes the dynamic model of the manipulator and perturbation derived from the dynamics. In Section 3, the SPO-based reaction force estimation method is introduced. In Section 4, the estimated reaction force is evaluated through a simulation. In Section 5, the implementation and experiment results are presented. Section 6 concludes the work.

2. DYNAMIC MODELLING AND PERTURBATION

The dynamics of a robot describe the relationship between forces, torques, and motion. The general dynamic equation of a manipulator in free space is:

$$T = A(\theta)\,\ddot{\theta} + B\left(\theta,\dot{\theta}\right) + g(\theta), \tag{1}$$

where θ, $A(\theta)$, $B(\theta,\dot{\theta})$, $g(\theta)$, and T are the vector joint of the angles, mass/inertia matrix, centrifugal/Coriolis torque, gravity torque in joint space, and vector of the joint torques, respectively. The dynamics of the robot is based on revolute joints. The masses of the links are considered to be uniformly distributed throughout the entire length. The mass of each link is concentrated at the geometrical center. The masses of the links and actuators are denoted by m_1, m_2, m_3, and l_1, l_2, l_3 denote the lengths of each link. The joint torques and positions of the robot are defined as T_1, T_2, T_3 and θ_1, θ_2, θ_3, respectively.

The dynamic equations of robots are developed using Lagrange's equation

$$T_1 = A_1 + \psi_1, \tag{2}$$
$$T_2 = A_2 + \psi_2, \tag{3}$$
$$T_3 = A_3 + \psi_3, \tag{4}$$

where A_1, A_2, and A_3 are defined

$$A_1 = [\frac{1}{3}m_1l_1^2 + m_2(l_1^2 + \frac{1}{3}l_2^2) + m_3(l_1^2 + l_2^2 + \frac{1}{3}l_3^2)]\ddot{\theta}_1$$

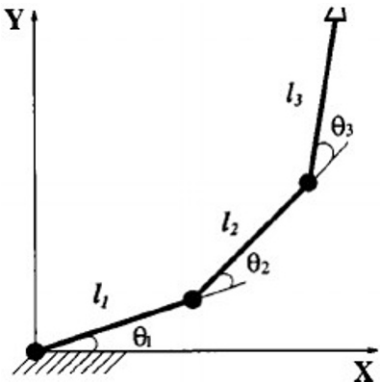

Fig. 1. The three-link manipulator.

$$+[\frac{1}{3}m_2l_2^2 + \frac{1}{2}m_3(2l_2^2 + \frac{2}{3}l_3^2)]\ddot{\theta}_2 + [\frac{1}{3}m_3l_3^2)]\ddot{\theta}_3, \tag{5}$$

$$A_2 = [\frac{1}{3}m_2l_2^2 + \frac{1}{2}m_3(2l_2^2 + \frac{2}{3}l_3^2)]\ddot{\theta}_1 + [\frac{1}{3}m_2l_2^2 + m_3(l_2^2 + \frac{1}{3}l_3^2)]\ddot{\theta}_2 + [\frac{1}{3}m_3l_3^2)]\ddot{\theta}_3, \tag{6}$$

$$A_3 = [\frac{1}{3}m_3l_3^2]\ddot{\theta}_1 + [\frac{1}{3}m_3l_3^2]\ddot{\theta}_2 + [\frac{1}{3}m_3l_3^2]\ddot{\theta}_3. \tag{7}$$

Perturbation is defined as the combination of all the uncertainties. The perturbations derived from the dynamics of the robot are:

$$\begin{aligned}\psi_1 = {} & [m_2l_1l_2c_2 + m_3(2l_1l_2c_2 + l_1l_3c_{23} + l_2l_3c_3)]\ddot{\theta}_1 \\ & + [\frac{1}{2}m_2l_1l_2c_2 \\ & + \frac{1}{2}m_3(2l_1l_2c_2 + l_1l_3c_{23} + 2l_2l_3c_3)]\ddot{\theta}_2 \\ & + [\frac{1}{2}m_3(l_1l_3c_{23} + l_2l_3c_3)]\ddot{\theta}_3 \\ & + [-m_2l_1l_2s_2 - m_3(2l_1l_2s_2 + l_2l_3s_3)]\dot{\theta}_1 \\ & + [-\frac{1}{2}m_2l_1l_2s_2 + \frac{1}{2}m_3(-2l_1l_2s_2 - 2l_2l_3s_3)]\dot{\theta}_2 \\ & + [-\frac{1}{2}m_3l_2l_3s_3]\dot{\theta}_3 + \frac{1}{2}m_1gl_1c_1 \\ & + m_2g(l_1c_1 + \frac{1}{2}l_2c_{12}) \\ & + m_3g(l_1c_1 + l_2c_{12} + \frac{1}{2}l_3c_{123}),\end{aligned} \tag{8}$$

$$\begin{aligned}\psi_2 = {} & [\frac{1}{2}m_2l_1l_2c_2 + \frac{1}{2}m_3(2l_1l_2c_2 + l_1l_3c_{23} \\ & + 2l_2l_3c_3)]\ddot{\theta}_1 + [m_3l_2l_3c_3]\ddot{\theta}_2 + [\frac{1}{2}m_3l_2l_3c_3]\ddot{\theta}_3 \\ & + [-\frac{1}{2}m_2l_1l_2s_2 - m_3(l_1l_2s_2 + l_2l_3s_3)]\dot{\theta}_1 \\ & + [-m_3l_2l_3s_3]\dot{\theta}_2 + [-\frac{1}{2}m_3l_2l_3s_3]\dot{\theta}_3 + [\frac{1}{2}m_2l_1l_2s_2 \\ & + \frac{1}{2}m_3(2l_1l_2s_2 + l_1l_3s_{23})]\dot{\theta}_1^2 + [\frac{1}{2}m_2l_1l_2s_2\end{aligned}$$

$$+\frac{1}{2}m_3(2l_1l_2s_2+l_1l_3s_{23})]\dot{\theta}_1\dot{\theta}_2 +[\frac{1}{2}m_3l_1l_3s_{23}]\dot{\theta}_1\dot{\theta}_3+\frac{1}{2}m_2gl_2c_{12} +m_3g(l_2c_{12}+\frac{1}{2}l_3c_{123}), \quad (9)$$

$$\psi_3=[\frac{1}{2}m_3(l_1l_3c_{23}+l_2l_3c_3)]\ddot{\theta}_1+[\frac{1}{2}m_3l_2l_3c_3]\ddot{\theta}_2 +[-\frac{1}{2}m_3l_2l_3s_3]\dot{\theta}_1+[-\frac{1}{2}m_3l_2l_3s_3]\dot{\theta}_2 +[\frac{1}{2}m_3(l_1l_3s_{23}+l_2l_3s_3)]\ddot{\theta}_1^2+[\frac{1}{2}m_3l_2l_3s_3]\dot{\theta}_2^2 +[\frac{1}{2}m_3(l_1l_3s_{23}+2l_2l_3s_3)]\dot{\theta}_1\dot{\theta}_2 +[\frac{1}{2}m_3(l_1l_3s_{23}+l_2l_3s_3)]\dot{\theta}_1\dot{\theta}_3 +[\frac{1}{2}m_3l_2l_3s_3]\dot{\theta}_2\dot{\theta}_3+\frac{1}{2}m_3gl_3c_{123}. \quad (10)$$

In these equations, ψ_1, ψ_2, $\psi_3$are the perturbations of link1, link2, and link3, respectively. Furthermore, $c=\cos$, $s=\sin$, $c_{12}=\cos(\theta_1+\theta_2)$, $c_{23}=\cos(\theta_2+\theta_3)$, $s_{23}=\sin(\theta_2+\theta_3)$, and $c_{123}=\cos(\theta_1+\theta_2+\theta_3)$.

3. SLIDING MODE CONTROL WITH SLIDING PERTURBATION OBSERVER (SMCSPO)

3.1. Design of SMCSPO

The actuators are controlled by SMC, and the reaction force is estimated by the SPO. The governing equation for general second-order dynamics with n degrees of freedom (DoF) is:

$$\ddot{x}_j=f_j(x)+\Delta f_j(x)+\sum_{i=1}^{n}[(b_{ji}(x)+\Delta b_{ji}(x))u_i] +d_j(t), \quad (11)$$

where $x\triangleq[X_1...X_n]^T$is the state vector, and $X_j\triangleq[x_j,\dot{x}_j]^T$. The terms $f_j(x)$ and $\Delta f_j(x)$ correspond to the nonlinear driving terms and their uncertainties. The components b_{ji} and Δb_{ji} represent the elements of the control gain matrix and their uncertainties, d_j is the external disturbance, and u_j is the control input. The terms f_j and b_{ji} are known continuous functions of the state [44]. The estimated perturbation is defined as the combination of all uncertainties. The estimated and actual sliding functions are:

$$\hat{s}=\dot{\hat{e}}+c\hat{e}, \quad (12)$$

$$s=\dot{e}+ce, \quad (13)$$

where $c>0$, and $\hat{e}=\hat{\theta}-\theta_{dj}$ is the estimated position tracking error. $e=\theta-\theta_{dj}$ is the actual position tracking error. The robustness of the controller is confirmed using Lyapunov stability theory. The Lyapunov function candidate (attractive condition) is defined as follows:

$$\dot{V}(\hat{s}_j)=\hat{s}_j\dot{\hat{s}}_j<0, \quad (14)$$

where $\hat{s}$ and $\dot{\hat{s}}$ are:

$$\hat{s}_j=\hat{\theta}_{2j}-(k_{1j}/\varepsilon_{0j})\tilde{\theta}_{1j}-\dot{\theta}_{jd}+c\left(\hat{\theta}_{1j}-\theta_{jd}\right), \quad (15)$$

$$\dot{\hat{s}}=\alpha_3\bar{u}_i-\left[k_{2j}/\varepsilon_{0j}+c(k_{1j}/\varepsilon_{0j})-(k_{1j}/\varepsilon_{0j})^2\right]\tilde{\theta}_{1j} -(k_{1j}/\varepsilon_{0j})\tilde{\theta}_{2j}-\ddot{\theta}_{jd}+c\left(\hat{\theta}_{2j}-\dot{\theta}_{jd}\right)+\hat{\psi}_i. \quad (16)$$

The proof is shown in the appendix A.

The control $\bar{u}_i$ is selected to enforce $\dot{\hat{s}}\hat{s}<0$ outside a prescribed manifold. The desired $\hat{s}$-dynamics is selected as:

$$\dot{\hat{s}}=-Ksat(\hat{s}), \quad (17)$$

$$sat(\hat{s})=\begin{cases}\hat{s}/|\hat{s}|, & \text{if } |\hat{s}|\geq\varepsilon,\\ \hat{s}\varepsilon, & \text{if } |\hat{s}|\leq\varepsilon,\end{cases} \quad (18)$$

where ε is the boundary layer of the SMC controller, and K is the robust control gain. The equations of SPO for link1, link2, and link3 are derived as follows:

$$\dot{\hat{\theta}}_{1j}=\hat{\theta}_{2j}-k_{1j}sat(\tilde{\theta}_{1j}), \quad (19)$$

$$\dot{\hat{\theta}}_{2j}=\alpha_{3j}\bar{u}_i-k_{2j}sat(\tilde{\theta}_{1j})+\hat{\psi}_i, \quad (20)$$

$$\dot{\hat{\theta}}_{3j}=\alpha_{3j}^2(\bar{u}_i-\hat{\theta}_{3j}+\alpha_{3j}\hat{\theta}_{2j}), \quad (21)$$

$$\hat{\psi}_i=\alpha_{3j}(\alpha_3\hat{\theta}_{2j}-\hat{\theta}_{3j}), \quad (22)$$

$$\bar{u}_i=\frac{1}{\alpha_{3j}}\{-K_jsat(\hat{s}_j)\}+\frac{1}{\alpha_{3j}}\{-(\frac{k_{ij}}{\varepsilon_{0j}})\tilde{\theta}_{2j} +[\frac{k_{2j}}{\varepsilon_{0j}}+c_{1j}\frac{k_{1j}}{\varepsilon_{0j}}-(\frac{k_{1j}}{\varepsilon_{0j}})^2]\tilde{\theta}_{1j}+\ddot{\theta}_{jd} -c_{1j}(\hat{\theta}_{2j}-\dot{\theta}_{jd})-\hat{\psi}_i\}, \quad (23)$$

$i,\ j=1,\ 2,\ 3,$

where k_{1j}, k_{2j}, α_{3j} are positive numbers, $\tilde{\theta}=\hat{\theta}-\theta$ is the estimation error of the measurable state, $\hat{\theta}$ is the estimated value, and θ is the actual value. $\hat{\psi}_i$ is the estimated perturbation for link1, link2, and link3. Throughout the text, "~" refers to estimation errors, whereas "^" indicates an estimated quantity.

The actual s-dynamics within the boundary layer $|\hat{s}|\leq\varepsilon_{0j}$ becomes

$$\dot{s}+\frac{K_j}{\varepsilon_{0j}}s=\left[\frac{k_{2j}}{\varepsilon_{0j}}-\left(\frac{k_{1j}}{\varepsilon_{0j}}-\frac{K_j}{\varepsilon_{0j}}\right)\left(c-\frac{k_{1j}}{\varepsilon_{0j}}\right)\right]\tilde{\theta}_{1j} -\left(c+\frac{K_j}{\varepsilon_{0j}}\right)\tilde{\theta}_{2j}-\hat{\psi}_i. \quad (24)$$

Once $\left|\tilde{\theta}_{1j}\right|\leq\varepsilon_{0j}$ and $|\hat{s}|\leq\varepsilon_{0j}$ are reached, i.e., the double sliding is in effect, the observer and s-dynamics become:

$$\begin{bmatrix}\dot{\tilde{\theta}}_{1j}\\ \dot{\tilde{\theta}}_{2j}\\ \dot{\tilde{\theta}}_{3j}\\ \dot{s}\end{bmatrix}$$

$$= \begin{bmatrix} -k_{1j}/\varepsilon_{0j} & 1 & 0 & 0 \\ -k_{2j}/\varepsilon_{0j} & \alpha_{3j}^2 & -\alpha_{3j} & 0 \\ 0 & \alpha_{3j}^3 & -\alpha_{3j}^2 & 0 \\ k_{2j}/\varepsilon_{oj} & & & \\ -(c-k_{1j}/\varepsilon_{0j})^2 & -(2c+\alpha_{3j}^2) & \alpha_{3j} & -c \end{bmatrix} \times \begin{bmatrix} \tilde{\theta}_{1j} \\ \tilde{\theta}_{2j} \\ \tilde{\theta}_{3j} \\ s \end{bmatrix} + \begin{bmatrix} 0 \\ 0 \\ 1 \\ 0 \end{bmatrix} \psi_i/\alpha_{3j}. \quad (25)$$

The associated characteristic equation is:

$$[\lambda + c] \times \left[\lambda^3 + (k_{1j}/\varepsilon_{0j})\lambda^2 + (k_{2j}/\varepsilon_{0j})\lambda + \alpha_{3j}^2 (k_{2j}/\varepsilon_{0j})\right] = 0. \quad (26)$$

This leads to the following design solution:

$$\begin{aligned} k_{1j}/\varepsilon_{0j} &= 3\lambda_d, \\ k_{2j}/k_{1j} &= \lambda_d, \\ \alpha_{3j} &= \sqrt{\lambda_d/3}, \\ c = K_j/\varepsilon_{0j} &= \lambda_d. \end{aligned} \quad (27)$$

3.2. Estimation of reaction force using sliding perturbation observer

Before integrating the SPO into the SMC, it is convenient to decouple the control variable using the following transformation [45]:

$$f_j(\hat{x}) + \sum_{i=1}^{n} b_{ji}(\hat{x})\, u_i = \alpha_{3j}\bar{u}_j, \quad (28)$$

where $\alpha_{3j}$is an arbitrary positive number, and $\bar{u}_j$is the new control variable. The original control vector of general equation is obtained as:

$$u = B^{-1} Col[\alpha_{3j}\bar{u}_j - f_j(\hat{x})], \quad (29)$$

where $u = [u_1 .... u_n]^T$ and $B = [b_{ji}(\hat{x})]_{n\times n}$. This transformation allows us to write the system dynamics as:

$$\ddot{x}_j = \alpha_{3j}\bar{u}_j + \psi_j. \quad (30)$$

The state space representation of (30) and corresponding SO structure are:

$$\begin{aligned} \dot{\theta}_{1j} &= \theta_{2j}, \\ \dot{\theta}_{2j} &= \alpha_{3j}\bar{u}_j + \psi_j, \quad (31) \\ \dot{\hat{\theta}}_{1j} &= \hat{\theta}_{2j} - k_{1j} sat(\tilde{\theta}_{1j}) - \alpha_{1j}\tilde{\theta}_{1j} < \quad (32) \\ \dot{\hat{\theta}}_{2j} &= \alpha_{3j}\bar{u}_i - k_{2j} sat(\tilde{\theta}_{1j}) - \alpha_{2j}\tilde{\theta}_{1j}. \quad (33) \end{aligned}$$

A new state variable θ_{3j} is defined in order to focus on the perturbation estimation aspects.

$$\theta_{3j} = \alpha_{3j}\theta_{2j} - \Psi/\alpha_{3j}. \quad (34)$$

The time derivative of (35) is:

$$\dot{\theta}_{3j} = \alpha_{3j}\dot{\theta}_{2j} - \dot{\Psi}/\alpha_{3j}. \quad (35)$$

The new observer error dynamics becomes:

$$\dot{\tilde{\theta}}_{3j} = \alpha_{3j}^2\left(-\tilde{\theta}_{3j} + \alpha_{3j}\tilde{\theta}_{2j}\right) + \dot{\Psi}/\alpha_{3j}. \quad (36)$$

The reaction force can be calculated to estimate the value of the perturbation using an SPO-based algorithm. The estimated perturbation includes the external disturbance forces, errors in the dynamics, and gravitational non-liner terms. In assembly work, the motion is usually slow. If the motion is slow, then nonlinear terms with velocity or acceleration such as inertia and Coriolis terms become zero, so only disturbance remains as the estimated perturbation. Therefore, the reaction force becomes the estimated perturbation, which can be found using SPO.

4. SIMMECHANICS-BASED SIMULATION

The reaction force of the end effector using the SPO algorithm was evaluated through simulation. Simulation results are provided for the cases below:

I) The estimated perturbation of the end effector without external force and without collision (see Fig. 6).

II) The estimated perturbation of the end effector with external force but without collision (see Fig. 10).

III) The estimated perturbation of the end effector with collision (see Fig. 12).

IV) The estimated perturbation of the end effector with external force in rise and fall condition (see Fig. 15).

4.1. Model of the three-link dual-arm manipulator

A model the manipulator was designed in SolidWorks and then transferred to the SimMechanics tool box. SimMechanics allows us to verify model-based control algorithms [46]. The simulation of the manipulator was done using MATLAB/SIMULINK. Fig. 2 shows a block diagram of the SMCSPO scheme. The model of the manipulator is shown in Fig. 3.

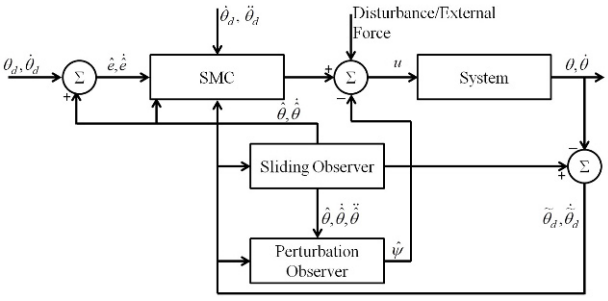

Fig. 2. Block diagram of control algorithm (SMCSPO).

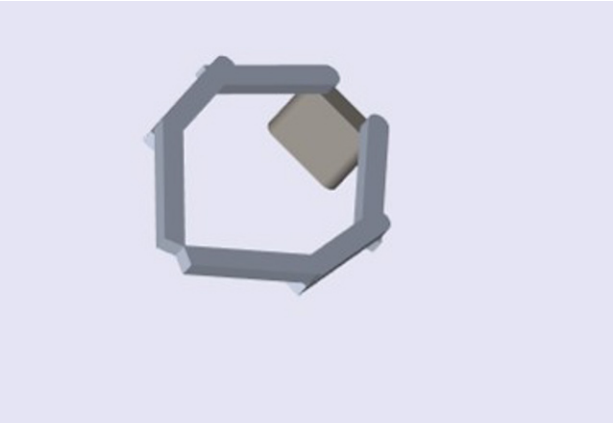

Fig. 3. Three Link dual arm robot manipulator.

Table 1. Model parameter used in simulation.

	Parameters	Values
(1)	m_1,m_2,m_3	0.343085 kg
(2)	l_1,l_2,l_3	0.2m
(3)	g	9.81 m/s^2

Table 2. Design parameter of SMCSPO.

	Parameters	Values
(1)	K	28
(2)	k_1	24
(3)	k_2	192
(4)	α_3	1.63299
(5)	ε_0	1
(6)	c	8
(7)	e	3.5

4.2. Simulation results

The estimated reaction force was evaluated by simulation. The model parameters used in the simulation are listed in Table 1. Table 2 shows the design parameters of SMCSPO.

Fig. 4 shows the real and desired trajectories of end effector without collision. Fig. 5 shows error between trajectories.

Fig. 6 shows the estimated perturbation of the end effector without external force and without collision. In the beginning when the input trajectory increases, there is a very small estimated perturbation observed from the SPO in the system, but it goes to zero after 8 seconds, when there is no external force. The reason for this is the initial error between the real trajectory and desired trajectory when the system starts moving, as shown in Fig. 5. It is also due to the initial rapid start of the input trajectory, which is almost exponentially increasing from 0 to 8 seconds. Additionally, the system is affected by external

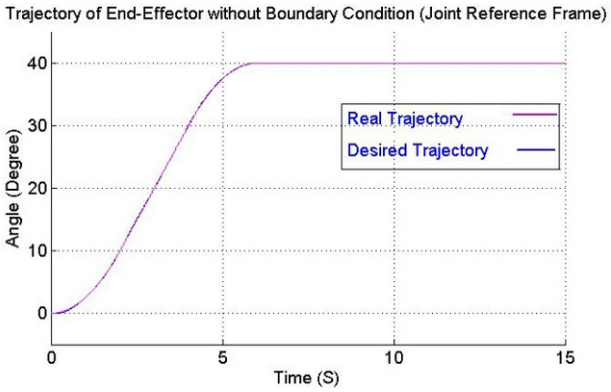

Fig. 4. Input trajectory of end effector.

Fig. 5. Error between trajectories.

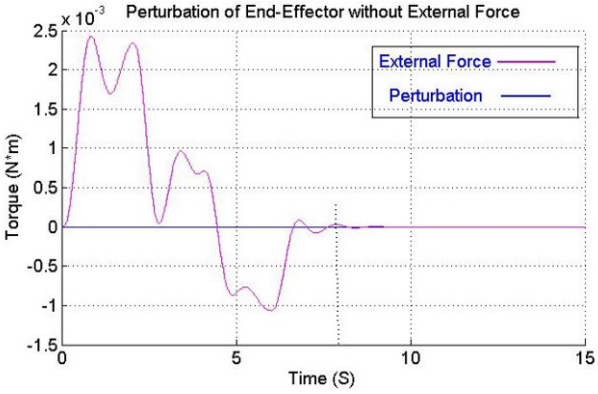

Fig. 6. Estimated perturbation of end effector without external force.

disturbance. However, this estimated perturbation (from 0 to 8 seconds) is very small and can be neglected. After 8 seconds, the estimated perturbation is almost equal to the assumed real perturbation.

Fig. 7 shows the real and desired trajectories and the error of the trajectories of the end effector with external force but without collision. External force is generated by using the joint sensor of the end effector. When the input trajectory is greater than 36.5 degrees, the external force

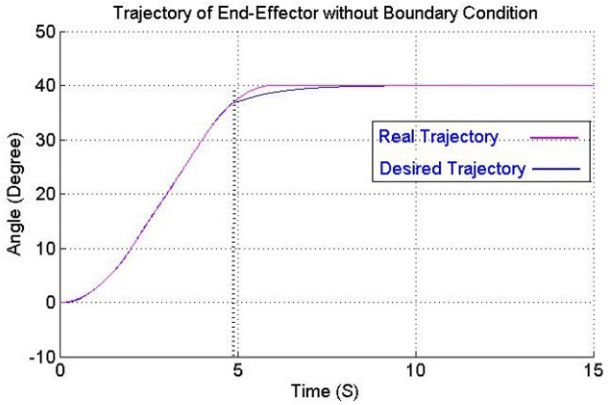

Fig. 7. Real and desired trajectories of end effector.

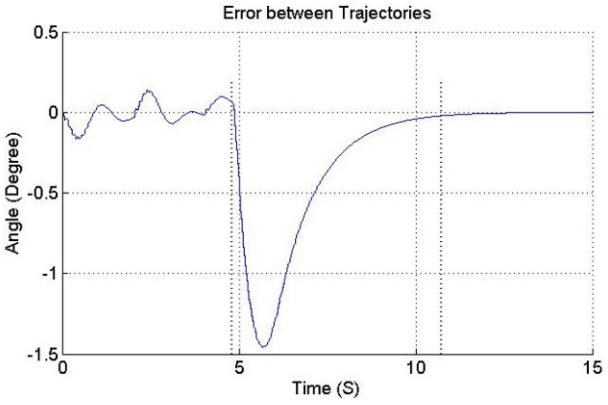

Fig. 8. Error between trajectories.

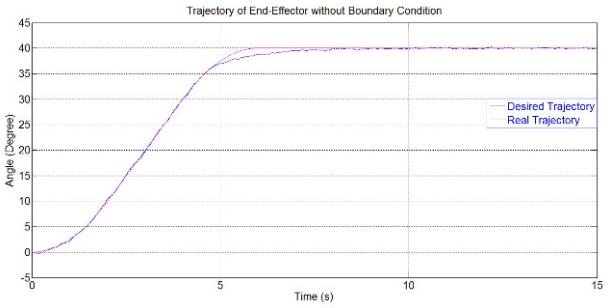

Fig. 9. Real and desired trajectories of end effector.

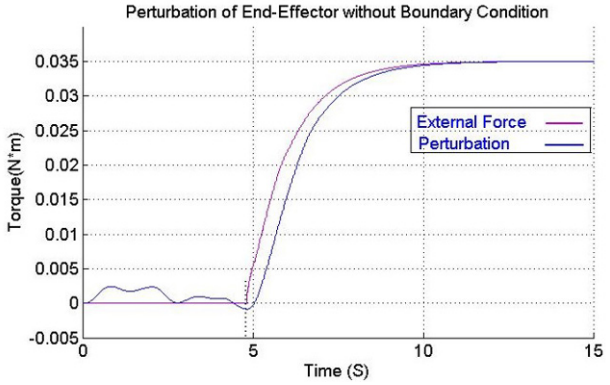

Fig. 10. Estimated perturbation of end effector without collision.

is applied. External force is applied at the joint actuator of the end effector. At the beginning when external force is applied, the error between the desired and real trajectories is almost 1.5 degrees. The error becomes zero after 4 seconds of external force (i.e., at 9 seconds), and then the desired trajectory follows the real trajectory. Fig. 8 shows the error between trajectories.

To show the effect of additive noise on the performance of the closed-loop system, we added a random signal (from a uniform random number block) to our Simulink model. The uniform random number block generates uniformly distributed random numbers over an interval of 0.08 and -0.08. The starting seed for the random number is zero. The output is repeatable for a given seed. The time interval between samples is 0.1. The simulation result with additive noise is shown in Fig. 9, which shows that the control performance is still very good., and the desired trajectory is achieved at the same time as in the case without noise (Fig. 7). Some disturbance in the response shows the sensor noise in Fig. 9.

For the first 4 seconds when there is no external force, the estimated perturbation observed form the SPO is also very small (near zero). When the external force increases, the estimated perturbation observed from the SPO also increases but with some phase difference. Fig. 10 shows the estimated perturbation of the end effector with external force but without collision. The maximum reaction force from the observer is 0.035 N*m when the end effector reaches its desired position.

Fig. 11 shows the real and desired trajectories of the end effector with collision. The real trajectory changes when the end effectors collide with each other. The end effectors of the manipulators cannot go forward after they collide with each other. After 5 seconds, when the angle is greater than 37 degrees, the trajectories changed because of the collision.

The reaction force of the end effector increases when the external force is increased. Fig. 12 shows the estimated perturbation of the end effector after collision. After 5 seconds, when the angle of the desired trajectory is greater than 37 degrees, oscillation in the external forced is observed due to the collision of the end effector. However, after 10 seconds (Fig. 12), the difference between the estimated perturbation and real perturbation becomes negligible. The difference is zero because the external force is zero after 10 seconds (Fig. 12).

Fig. 13 shows the real and desired trajectories and error of the trajectories of the end effector with external force in rising and falling conditions. In this case, when the end effectors collide, the external force is not removed. At the

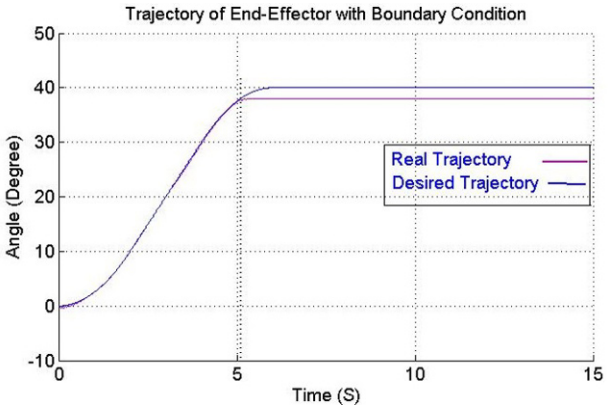

Fig. 11. Real and desired trajectories of end effector with collision.

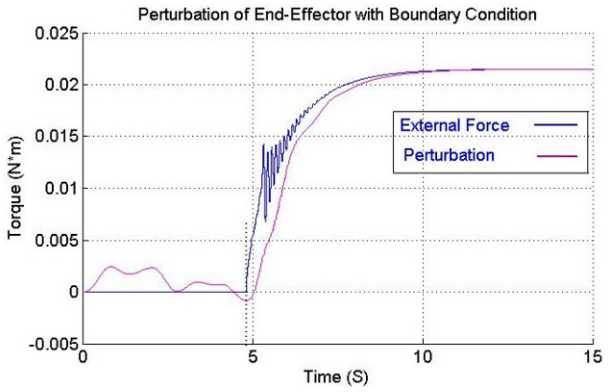

Fig. 12. Estimated perturbation of end effector with collision.

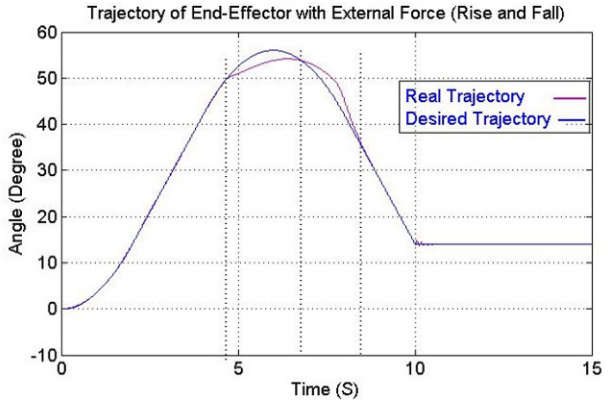

Fig. 13. Real and desired trajectories of end effector with rise and fall condition.

point of collision, the external force is increased (i.e., rising conditions), which causes the desired trajectory to follow the real trajectory but with some error. At 7 seconds, the external force is removed (i.e., falling conditions). After this, the desired trajectory follows the real trajectory. Fig. 14 shows the error between trajectories.

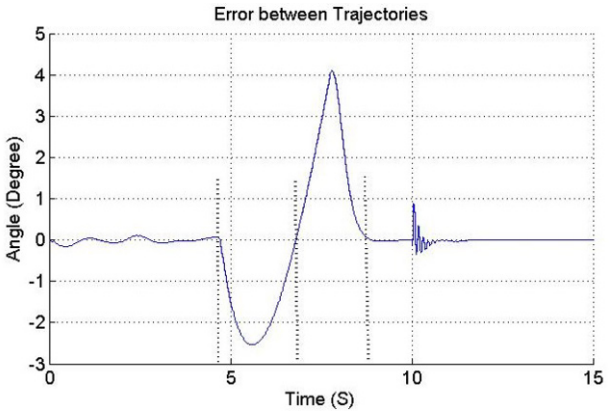

Fig. 14. Error between trajectories.

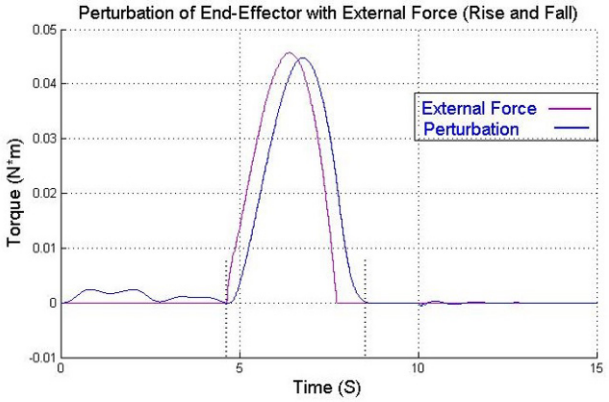

Fig. 15. Estimated perturbation of end effector with rise and fall condition.

In the rising conditions, when the external force increases, the estimated perturbation also increases and reaches its maximum value, but with some phase difference due to the initially applied external force. In the falling conditions, when the external force decreases, the estimated perturbation also decreases. The estimated perturbation goes to zero when there is no external force exists. The effect is shown in Fig. 15.

5. IMPLEMENTATION AND EXPERIMENTS

The experiment setup is shown in Fig. 16, which includes a 3DOF manipulator. Due to the limitation of the experimental setup, we could only perform experiments for case IV. The experimental result is provided in Fig. 16, which matches the simulation result shown in Fig. 15. The proposed algorithm was implemented on a three-link hydraulic servo system instead of a three-link dual-arm manipulator. Previous studies examined the identification and robust control of a hydraulic servo system [47, 48]. The system consists of two hydraulic cylinders and one AC servo motor, as shown in Fig. 16.

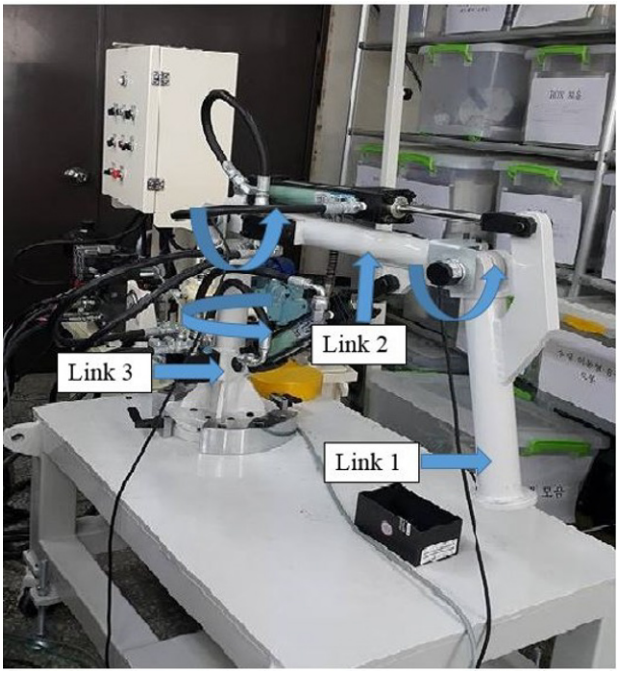

Fig. 16. Structure of three link hydraulic servo system.

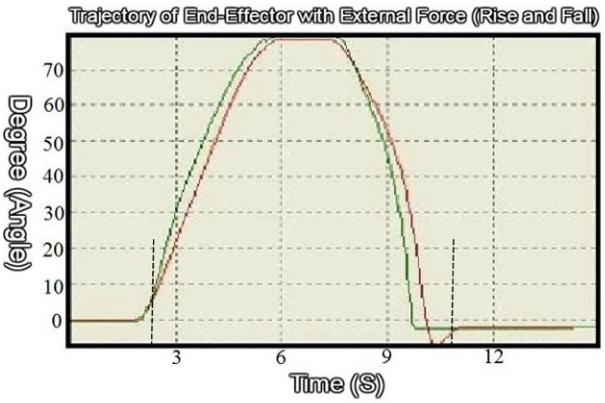

Fig. 17. Experimental result of real and desired trajectories of end effector with rise and fall condition.

Fig. 17 shows the experimental result of the real and desired trajectories of the end effector with external force in rising and falling conditions. The real trajectory is shown as a green line, and the desired trajectory is shown as a red line.

Fig. 18 shows the experimental result of the estimated perturbation of the end effector with external force in rising and falling conditions. In the rising conditions, when the external force increases, the estimated perturbation also increases and reaches its maximum value. In the falling conditions, when the external force decreases, the estimated perturbation also decreases. The estimated perturbation goes to zero when there is no external force.

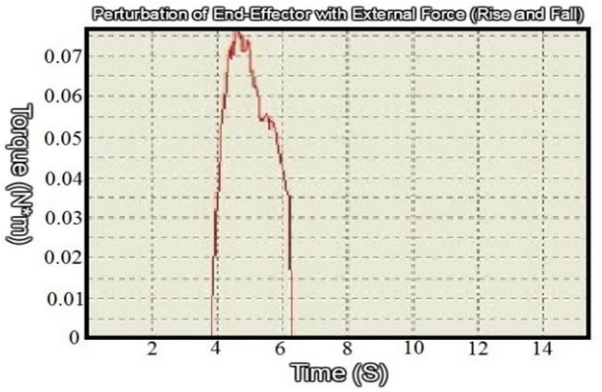

Fig. 18. Experimental result of estimated perturbation of end effector with rise and fall condition.

6. CONLUSION

This research introduced an estimation method of the reaction force of the end effector of a three-links dual-arm robot manipulator using SMCSPO without using any force sensor. The proposed method is based on previous research [49]. Unlike the previous research, the perturbation includes external force, the interactive force of the manipulator, viscous friction, Coulomb friction, and model parameter error of the mass, which can affect the reaction force estimation. The estimated perturbation has low accuracy compared to the force estimation sensor, and it is difficult to measure very low reaction force. However, it is useful to find the reaction force when we cannot use a sensor, such as in the transportation of active uranium in nuclear power plants, disposal of explosive ordnance, remote cutting for dismantling nuclear power plants, deburring, welding, and grinding. In future research, other factors may also be included to improve the accuracy of force estimation.

APPENDIX A

Perturbation is defined as the combination of all the uncertainties of (11)

$$\psi_j(x,t) = \Delta f_j(x) + \sum_{i=1}^{n}[\Delta b_{ji}(x)\,u_i] + d_j(t)\,. \qquad (A.1)$$

It is assumed that the perturbations are upper bounded by a known continuous function of the state (Elmali and Olgac, 1992)

$$\Gamma_j(x,t) = F_j(x) + \Sigma\,|\Phi_{ji}^{n}(x)\,u_i| + D_j(t) > |\Psi_j(t)|\,, \qquad (A.2)$$

where $F_j > |\Delta f_j|$, $\Phi_{ji} > |\Delta b_{ji}|$ and $D_j > |d_j|$ represent the expected upper bounds of the uncertainties. The condi-

tions for the existence of sliding mode are:

$$\tilde{\theta}_2 \le k_1 + \alpha_1 \tilde{\theta}_1 \left(if \tilde{\theta}_1 > 0\right),$$
$$\tilde{\theta}_2 \ge -k_1 + \alpha_1 \tilde{\theta}_1 \left(if \tilde{\theta}_1 < 0\right). \quad (A.3)$$

The error dynamics take the form of:

$$\dot{\tilde{\theta}}_2 + \left(k_1/k_2\right)\tilde{\theta}_2 = -\Psi. \quad (A.4)$$

The stability of the SPO is guaranteed by setting $k_2 \ge \Gamma_j(x,t)$, which assures that $\left|\tilde{\theta}_2\right| \le k_1$ in steady state, as can be seen in (A.4). This implies that the sliding conditions (A.3) are also verified. The expression for k_2 should be based on $\hat{\theta}$. We assume that $\Gamma_j(x,t)$ is also an upper bound of Ψ, meaning that the uncertainties due to the state estimation are negligible compared to the modeling uncertainties and external disturbances.

Closed-loop stability is defined using Lyapunov stability theory. $\dot{\hat{s}}\hat{s} < 0$ is derived as the following equation.

$$\begin{aligned}
&-\left[\left(k_{1j}/\varepsilon_{0j}\right)\tilde{\theta}_{1j} + \dot{\theta}_{jd} - \hat{\theta}_{2j} - c\left(\hat{\theta}_{1j} - \theta_{jd}\right)\right]\alpha_3\bar{u}_j \\
&-\left[k_{2j}/\varepsilon_{0j} - \left(k_{1j}/\varepsilon_{0j}\right)^2 + 2c\left(k_{1j}/\varepsilon_{0j}\right)\right]\tilde{\theta}_{1j}\hat{\theta}_{2j} \\
&-\left[\left(k_{1j}/\varepsilon_{0j}\right)^3 - k_{1j}k_{2j}/\left(\varepsilon_{0j}\right)^2 - c\left(k_{1j}/\varepsilon_{0j}\right)^2\right]\left(\tilde{\theta}_{1j}\right)^2 \\
&-\left[\left(k_{1j}/\varepsilon_{0j}\right)^2 - k_{2j}/\varepsilon_{0j} - 2c\left(k_{1j}/\varepsilon_{0j}\right)\right]\tilde{\theta}_{1j}\dot{\theta}_{jd} \\
&-\left[k_{2j}/\varepsilon_{0j} - \left(k_{1j}/\varepsilon_{0j}\right)^2 + c\left(k_{1j}/\varepsilon_{0j}\right)\right]c\tilde{\theta}_{1j}\hat{\theta}_{1j} \\
&-\left[\left(k_{1j}/\varepsilon_{0j}\right)^2 - k_{2j}/\varepsilon_{0j} - c\left(k_{1j}/\varepsilon_{0j}\right)\right]\tilde{\theta}_{1j}\theta_{jd} \\
&-\left[\left(k_{1j}/\varepsilon_{0j}\right)\tilde{\theta}_{1j} - \hat{\theta}_{2j} + \dot{\theta}_{jd} + c\left(\hat{\theta}_{1j} - \theta_{jd}\right)\right] \\
&\times\left[\left(k_{1j}/\varepsilon_{0j}\right)\tilde{\theta}_{2j}\right] + c\left(\hat{\theta}_{2j}\right)^2 + c^2\dot{\theta}_{jd}\theta_{jd} \\
&-\left[2c\dot{\theta}_{jd} - c^2\hat{\theta}_{1j} + c^2\theta_{jd} + \ddot{\theta}_{jd} + \hat{\Psi}_i\right]\hat{\theta}_{2j} \\
&-\left[c\dot{\theta}_{jd} + \ddot{\theta}_{jd} - \hat{\Psi}_i\right]c\hat{\theta}_{1j} \\
&+\left[\left(k_{1j}/\varepsilon_{0j}\right)\tilde{\theta}_{1j} + \dot{\theta}_{jd} + c\theta_{jd}\right]\ddot{\theta}_{jd} \\
&-\left[\left(k_{1j}/\varepsilon_{0j}\right)\tilde{\theta}_{1j} + \dot{\theta}_{jd} + c\theta_{jd}\right]\hat{\Psi}_i \\
&< 0. \quad (A.5)
\end{aligned}$$

The control $\bar{u}_i$ is selected to enforce $\dot{\hat{s}}\hat{s} < 0$ outside a prescribed manifold.

$$\begin{aligned}
\bar{u}_i = &\frac{1}{\alpha_{3j}}\{-K_j sat(\hat{s}_j)\} + \frac{1}{\alpha_{3j}}\{-(\frac{k_{ij}}{\varepsilon_{0j}})\tilde{\theta}_{2j} \\
&+[\frac{k_{2j}}{\varepsilon_{0j}} + c_{1j}\frac{k_{1j}}{\varepsilon_{0j}} - (\frac{k_{1j}}{\varepsilon_{0j}})^2]\tilde{\theta}_{1j} \\
&+\ddot{\theta}_{jd} - c_{1j}(\hat{\theta}_{2j} - \dot{\theta}_{jd}) - \hat{\psi}_i\}. \quad (A.6)
\end{aligned}$$

Using the value of $\bar{u}_i$ in the above equation (e), we obtain:

$$\begin{aligned}
&-\left[\left(k_{1j}/\varepsilon_{0j}\right)\tilde{\theta}_{1j} + \dot{\theta}_{jd} - \hat{\theta}_{2j} - c\left(\hat{\theta}_{1j} - \theta_{jd}\right)\right] \\
&\times\left[-Ksat\left(\hat{s}_j\right) + \left(k_{1j}/\varepsilon_{0j}\right)\tilde{\theta}_{2j}\right. \\
&+\left\{k_{2j}/\varepsilon_{0j} + c\left(k_{1j}/\varepsilon_{0j}\right) - \left(k_{1j}/\varepsilon_{0j}\right)^2\right\}\tilde{\theta}_{1j} \\
&+\ddot{\theta}_{jd} - c\left(\hat{\theta}_{2j} - \dot{\theta}_{jd}\right) - \hat{\Psi}_i\Big] \\
&-\left[k_{2j}/\varepsilon_{0j} - \left(k_{1j}/\varepsilon_{0j}\right)^2 + 2c\left(k_{1j}/\varepsilon_{0j}\right)\right]\tilde{\theta}_{1j}\hat{\theta}_{2j} \\
&-\left[\left(k_{1j}/\varepsilon_{0j}\right)^3 - k_{1j}k_{2j}/\left(\varepsilon_{0j}\right)^2 - c\left(k_{1j}/\varepsilon_{0j}\right)^2\right]\left(\tilde{\theta}_{1j}\right)^2 \\
&-\left[\left(k_{1j}/\varepsilon_{0j}\right)^2 - k_{2j}/\varepsilon_{0j} - 2c\left(k_{1j}/\varepsilon_{0j}\right)\right]\tilde{\theta}_{1j}\dot{\theta}_{jd} \\
&-\left[k_{2j}/\varepsilon_{0j} - \left(k_{1j}/\varepsilon_{0j}\right)^2 + c\left(k_{1j}/\varepsilon_{0j}\right)\right]c\tilde{\theta}_{1j}\hat{\theta}_{1j} \\
&-\left[\left(k_{1j}/\varepsilon_{0j}\right)^2 - k_{2j}/\varepsilon_{0j} - c\left(k_{1j}/\varepsilon_{0j}\right)\right]\tilde{\theta}_{1j}\theta_{jd} \\
&-\left[\left(k_{1j}/\varepsilon_{0j}\right)\tilde{\theta}_{1j} - \hat{\theta}_{2j} + \dot{\theta}_{jd} + c\left(\hat{\theta}_{1j} - \theta_{jd}\right)\right] \\
&\times\left[\left(k_{1j}/\varepsilon_{0j}\right)\tilde{\theta}_{2j}\right] + c\left(\hat{\theta}_{2j}\right)^2 + c^2\dot{\theta}_{jd}\theta_{jd} \\
&-\left[2c\dot{\theta}_{jd} - c^2\hat{\theta}_{1j} + c^2\theta_{jd} + \ddot{\theta}_{jd} + \hat{\Psi}_i\right]\hat{\theta}_{2j} \\
&-\left[c\dot{\theta}_{jd} + \ddot{\theta}_{jd} - \hat{\Psi}_i\right]c\hat{\theta}_{1j} \\
&+\left[\left(k_{1j}/\varepsilon_{0j}\right)\tilde{\theta}_{1j} + \dot{\theta}_{jd} + c\theta_{jd}\right]\ddot{\theta}_{jd} \\
&-\left[\left(k_{1j}/\varepsilon_{0j}\right)\tilde{\theta}_{1j} + \dot{\theta}_{jd} + c\theta_{jd}\right]\hat{\Psi}_i \\
&< 0.
\end{aligned}$$

After simplification, we obtain:

$$\begin{aligned}
&-\left[\hat{\theta}_{2j} + c\left(\theta_{1j} - \theta_{jd}\right) - \dot{\theta}_{jd} - \left(k_{1j}/\varepsilon_{0j}\right)\tilde{\theta}_{1j}\right]Ksat\left(\hat{s}_j\right) \\
&-c\left(\dot{\theta}_{jd}\right)^2 + c\hat{\theta}_{1j} - \hat{\Psi}_i\hat{\theta}_{2j} \\
&< 0.
\end{aligned}$$

REFERENCES

[1] K. Ohishi, M. Miyazaki, M. Fujita, and Y. Ogino, "Force control without force sensor based on mixed sensitivity $H\infty$ design method," *Proc. of IEEE Int. Con. on Robotics and Automation*, pp. 1356-1361, 1992. [click]

[2] K. Ohishi, M. Miyazaki, M. Fujita, and Y. Ogino, "$H\infty$ observer based force control without force sensor," *Proceedings of IEEE Int. Con. on Industrial Electronics, Control and Instrumentation*, pp. 1049-1054, 1991.

[3] K. Ohishi, M. Miyazaki, and M. Fujita, "Hybrid control of force and position without force sensor," *Proceedings of IEEE Int. Con. on Industrial Electronics, Control and Instrumentation*, pp.670-675, 1992.

[4] P. J. Hacksel and S. E. Salcudean, "Estimation of environment force and rigid-body velocities using observer," *Proc. of IEEE Int. Con. on Robotics and Automation*, pp. 93 1-936, 1994.

[5] T. Murakami, R. Nakamura, F. Yu, and K. Ohnishi, "Force sensorless impedance control by disturbance observer," *Record of the Power Conversion Conf.*, pp. 352-357, Apr. 1993.

[6] P. J. Hacksel and S. J. Salcudean, "Estimation of environmental forces and rigid-body velocities using observers," *Proc. of IEEE Conf. on Robotics and Automation*, pp. 931-936, 1994. [click]

[7] A. C. Smith and K. Hashtrudi-Zaad, "Application of neural networks in inverse dynamics based contact force estimation," *Proc. of IEEE Conf. on Control Applications*, pp. 1021-1026, Aug. 2005.

[8] V. Zahn, R. Maass, M. Dapper, and R. Eckmiller, "Learning friction estimation for sensorless force/position control in industrial manipulator," *Proc. of IEEE Conf. on Robotics and Automation*, pp. 2780-2785, May 1999.

[9] J. W. L. Simpson, C. D. Cook, and L. Zheng, "Sensorless force estimation for robots with friction," *Proc. of Australasian Conf. on Robotics and Automation*, Nov. 2002.

[10] M. Van Damme, P. Beyl, B. Vanderborght, V. Grosu, R. Van Ham, I. Van-derniepen, a. Matthys, and D. Lefeber. "Estimating robot end-effector force from noisy actuator torque measurements," *IEEE International Conf. on Robotics and Automation*, pp. 1108–1113, May 2011. [click]

[11] Z. Liu, F. Yu, L. Zhang, and T. Li, "Real-time estimation of sensorless planar robot contact information," *Journal of Robotics and Mechatronics*, vol. 29, no. 3, 2017. [click]

[12] N. Likar and L. Žlajpah, "External joint torque-based estimation of contact information," *The Int. J. of Advanced Robotic Systems*, vol. 11, pp. 1-11, 2014.

[13] L. D. Phong, J. Choi, and S. Kang, "External force estimation using joint torque sensors for a robot manipulator," *Proc. of IEEE International Conference on Robotics and Automation*, pp. 14-18, May 2012.

[14] L. Chan, F. Naghdy, and D. Stirling, "An improved extended active observer for adaptive control of a n−DOF robot manipulator," *J. Intell Robot System*, vol. 85, pp. 679-692, 2017. [click]

[15] J. Qin, F. Leonard, and G. Abba, "Experimental external force estimation using a non-linear observer for 6 axes flexible-joint industrial manipulators," *Proc. of 9th Asian Control Conference, ASCC*, Istanbul, Turkey, pp. 1-6, June 2013.

[16] S. Lichiardopol, N. V. de Wouw, and H. Nijmeijer. "Robust disturbance estimation for human–robotic manipulation," *Int. J. Robust Nonlinear Control*, vol. 24, pp. 1772-1796, 2014. [click]

[17] S. M. Yoon, W. J. Kim, and M. C. Lee, "Design of bilateral control for force feedback in surgical robot," *International Journal of Control, Automation, and Systems*, vol. 13, no. 4, pp. 916-925, 2015. [click]

[18] S. M. Yoon, M. C. Lee, and C. Y. Kim. "Sliding perturbation observer based reaction force estimation method of surgical robot instrument for haptic realization," *International Journal of Humanoid Robotics*, vol. 12, no. 2, pp. 1-19, 2015.

[19] J. Jung, J. Lee, and K. Huh, "Robust contact force estimation for robot manipulators in three-dimensional space," *Proc. of the Institution of Mechanical Engineers, Part C: Journal of Mechanical Engineering Science*, pp. 1317–1327, Sep. 2006.

[20] V. I. Utkin, "Variable structure systems with sliding modes," *IEEE Transactions on Automatic Control*, vol. 22, pp. 212-222, 1977. [click]

[21] N. Yagiz and Y. Hacioglu, "Fuzzy sliding modes with moving surface for robust control of a planar robot," *Journal of Vibration and Control*, vol. 11, no. 3, pp. 903-922, 2005

[22] P. Herman, "Sliding mode control of manipulators using first-order equations of motion with diagonal mass matrix," *Journal of the Franklin Institute*, vol. 342, pp. 353-363, 2005,

[23] M. L. Corradini and G. Orlando, "Control of mobile robots with uncertainties in dynamical model: a discrete time sliding mode approach with experimental results," *Control Engineering Practice*, vol. 10, pp. 23-34, 2002. [click]

[24] S. Yannier, A. Sabanovic, A. Onat, and M. Bastan, "Sliding mode based obstacle avoidance and target tracking for mobile robots," *Proceedings of the IEEE International Symposium on Industrial Electronics*, Dubrovnik, Croatia, pp. 1489-1494, June 2005.

[25] G. Herrmann, S. K. Spurgeon, and C. Edwards, "A model based sliding mode control methodology applied to the HDA-plant," *Journal of Process Control*, vol. 13, pp. 129-138, 2003. [click]

[26] E. M. Jafarov and R. Tasaltin, "Robust sliding mode control for the uncertain MIMO aircraft model F-18," *IEEE Transactions on Aerospace and Electronic Systems*, vol. 36, no. 4, pp. 1127-1141, 2000. [click]

[27] A. Jameel, M. Rehan, K. S. Hong, and N. Iqbal, "Distributed adaptive consensus control of Lipschitz nonlinear multi-agent systems using output feedback," *International Journal of Control*, vol. 89, no. 11, pp. 2336-2349, 2016. [click]

[28] M. Siddique and M. Rehan, "A concept of coupled chaotic synchronous observers for nonlinear and adaptive observers-based chaos synchronization," *Nonlinear Dyn.*, vol. 84, pp. 2251-2272, 2016. [click]

[29] S. Ahmad, M. Rehan and K. S. Hong, "Observer based robust control of one-sided Lipschitz non-linear systems," *ISA Transactions*, vol. 65, pp. 230-240, 2016. [click]

[30] S. Ahmad and M. Rehan, "On observer based control of one sided Lipschitz systems," *Journal of the Franklin Institue*, vol. 353, pp. 903-916, 2016.

[31] S. Nicosia and P. Tomei, "Robot control by using only joint position measurements," *IEEE Trans. Automat. Cont.*, pp. 1058-1061, Sep. 1990.

[32] W. H. Zhu, H. T. Chen and Z. J. Zhang, "A variable structure robot control algorithm with an observer," *IEEE Trans. Robotics Automat*, vol. 8, Aug. 1992.

[33] R. L. Hollis, S. Salcudean, and P. A. Allan, "A six degree-of-freedom magnetically levitated variable compliance fine motion wrist: design, modelling and control," *IEEE Trans. Robotics Automat*, vol. 7, pp. 320-332, June 1991. [click]

[34] S. R. Oh, R. L. Hollis, and S. Salcudean, "Precision assembly with a magnetically levitated wrist," *Proc. IEEE Conf. Robotics Automat.*, Atlanta, USA, pp. 127-134, May 1993.

[35] S. Salcudean, H. Davis, C. T. Chen, D. E. Goertz, and B. Tryggvason, "Coarse-fine residual gravity cancellation system with magnetic levitation," *Proc. IEEE Conf. Robotics Automat.*, Nice, France, pp. 10-15, May 1992.

[36] S. Salcudean, N. M. Wong, and R. L. Hollis, "A force-reflecting teleoperation system with magnetically levitated master and wrist," *Proc. IEEE Conf. Robotics Automat.*, Nice, France, pp. 10-15, May 1992.

[37] S. Salcudean, "A globally convergent angular velocity observer for rigid body motion," *IEEE Transactions on Automatic Control*, vol. 36, pp. 1493-1497, Dec. 1991. [click]

[38] C. H. An, C. G. Atkeson, and J. M. Hollerbach, *Model-based Control of a Robot Manipulator*, MIT Press, Cambridge, MA, 1988.

[39] Y. F. Zheng and J. Y. S. Luh, "Optimal load distribution for two industrial robots handling a single object," *Proc. of IEEE International Conference on Robotics and Automation*, Philadelphia, USA, pp. 344-349, 1988.

[40] P. Dauchez, X. Delebarre, Y. Bouffard, and E. Degoulange, "Task modeling and force control for a two-arm robot," *Proc. of IEEE International Conference on Robotics and Automation*, Sacramento, California, pp. 1702-1707, 1991.

[41] Q. Xue, A. A. Maciejewski, and P. C. Y. Sheu, "Determining the collision-free joint space graph for two cooperating robot manipulators," *IEEE Transactions on Systems, Man, and Cybernetics*, vol. 23, no. 1, pp. 285-294, 1993.

[42] A. Kron and G. Schmidt, "Haptic telepresent control technology applied to disposal of explosive ordnances: Principles and experimental results," *IEEE International Symposium on Industrial Electronics*, Dubrovnik, Croatia, pp. 1505-1510, 2005.

[43] N. Kimura, K. Ito, T. Fuji, and K. Fukimoto, "Mobile dual-arm robot for automated order picking system in warehouse containing various kinds of products," *Proc. of IEEE/SICE International Symposium on System Integration (SII)*, pp. 332-338, Dec. 2015.

[44] H. Elmali and N. Olgac, "Sliding mode control with perturbation estimation (SMCPE)," *International Journal of Control*, vol. 56, pp. 923-941, 1993. [click]

[45] M. J. Terra, H. Elmali, and N. Olgac, "Sliding mode control with perturbation observer," *J. Dyn. Syst. Measurement Control*, vol. 119, pp. 657-665, 1997. [click]

[46] L. T. Dung, H. J. Kang, and Y. S. Ro, "Robot manipulator modeling in Matlab-simmechanics with PD control and online gravity compensation," *IEEE. International Forum on Strategic Technology (IFOST)*, pp. 13-15, Oct. 2010.

[47] T. D. Cho, S. H. Seo, and S. M. Yang, "A study on the robust position control of single-rod hydraulic system," *Journal of the Korean Society of Precision Engineering*, vol. 16, no. 3, pp 128-135, 1999.

[48] M. Jelali and A. Kroll, *Hydraulic Servo-system: Modelling Identification and Control*, Springer Science & Business Media, 2012.

[49] S. M. Yoon, M. C. Lee, C. Y. Kim, and B. H. Kang, "Sliding perturbation observer based reaction force estimation method in surgical robot instrument," *Intelligent Robotics and Applications Lecture Notes in Computer Science*, vol. 8102, no. 1, pp. 227-236, 2013. [click]

Karam Dad Kallu is working towards a Ph.D. degree in Mechanical Engineering from Pusan National University, Busan, Korea since 2015. He received the M.S and B.S degrees in Mechatronics Engineering from Air University, Islamabad, Pakistan, in 2013 and 2011, respectively. His research interests include nonlinear control, adaptive control, robust control, robot manipulator and system identification.

Wang Jie received the B.S. degree in Mechanical Engineering from Pusan National University, Busan, Korea in 2015. His research interests include nonlinear control, adaptive control, robot manipulator, robust control and system identification.

Min Cheol Lee received the Ph.D. degree in Applied Physics from University of Tsukuba, Tsukuba, Japan in 1991, his M. Eng. Degree in Engineering Science from University of Tsukuba, Tsukuba, Japan in 1988, and his B.S. degree in Mechanical Engineering from Pusan National University, Busan, Korea in 1983. His research interests include intelligent robot control, autonomous mobile robot, signal processing to identify a system, robust control of a vehicle driving simulator, sensor application, mechatronics, measuring three dimensional distance and object configuration using vision information.